

Self-consistent evaluation of proximity and inverse proximity effects with pair-breaking in diffusive SN junctions

Arpit Raj,^{1,*} Patrick A. Lee,² and Gregory A. Fiete^{1,2}

¹*Department of Physics, Northeastern University, Boston, Massachusetts 02115, USA*

²*Department of Physics, Massachusetts Institute of Technology, Cambridge, MA 02139, USA*

We consider a planar superconducting-normal-metal (SN) junction with both inelastic and spin-flip scattering processes present. In the diffusive limit, we use a one-dimensional formulation of the Usadel equation to compute the self-consistent energy dependence of the single-particle density of states as a function of distance from the interface on both the superconducting and metallic sides for various spatial profiles of a pair-breaking spin-flip term. The pair-breaking processes fill in the superconducting gap at zero energy, which is reflected in the zero-bias tunneling conductance in scanning tunneling microscopy/spectroscopy experiments, in the vicinity of the junction. We also investigate the impact of having a partially transparent interface at the junction. We compare our findings with the observed exponential rise in the zero-bias conductance at the 1H step edge in recent experiments on 4Hb-TaS₂ [A. K. Nayak *et al.*, Nat. Phys. **17**, 1413 (2021)].

I. INTRODUCTION

When a superconductor (S) and a normal metal (N) are in close electrical contact, the metal can acquire superconducting correlations which can extend into the N side over a characteristic length scale, typically on the order of the superconducting coherence length. This is known as the proximity effect [1]. Conversely, the superconductivity on the S side of the system can be influenced by the presence of the normal metal, a phenomenon known as the inverse proximity effect, which can lead to a reduction in the superconducting gap close to the interface. Both effects can be important in hybrid superconductor-normal metal (SN) nanostructures [2]. The proximity and inverse proximity effects are influenced by factors such as the strength of the superconducting pairing, symmetry of the order parameter, spatial dimensionality of the two sides, and the quality of the SN interface. Understanding these effects is crucial for the design and optimization of superconducting devices and materials. Proximity effects are usually observed through a spatially varying local density of states (LDOS) across the interface and have been probed using local tunneling measurements, possible with a scanning tunneling microscope (STM), in the past [3–6].

On the theoretical side, proximity and inverse proximity effects in SN junctions are commonly studied in the diffusive limit using a quasiclassical theory governed by the Usadel equations [7]. This approach is particularly useful when the spatial dependence of the gap parameter and local density of states (LDOS) are of interest. Another advantage of this formalism is that it allows for a straightforward inclusion of both inelastic and spin-flip (pair-breaking) scattering processes by using the corresponding scattering rates, Γ_{in} and Γ_{sf} . While the inelastic scattering provides a

homogeneous energy broadening throughout the system (say, from thermal fluctuations in a system at uniform temperature), the spin-flip scattering can be highly position dependent. This may simply result, for instance, from presence of different magnetic impurities on the S and N sides. Surprisingly, although several authors have studied SN junctions using the Usadel equations in the past [3, 8–11], the effect of spatial profiles for Γ_{sf} has not been studied to the best of our knowledge.

We aim to bridge this gap by presenting a detailed study of the dependence of the superconducting gap Δ , zero-bias conductance (ZBC) and tunneling spectra across a diffusive SN junction on the strength and spatial profile of the spin-flip scattering for a range of parameters characterizing the materials and interface transparency. We employ a fully self-consistent solution of the Usadel equations to determine the proximity and inverse proximity effects. We also consider various limits that can be treated analytically.

A second impetus of this work is to revisit the differential tunneling conductance, dI/dV , spectra seen in recent STM experiments on the candidate topological superconductor 4Hb-TaS₂ [12] which is believed to have spin-flip scattering centers and SN junctions on surface step edges. The model we consider assumes a trivial superconducting state and thus it allows us to explore whether any of the experimental features can be captured without assuming the presence of topological boundary modes. Because unambiguous identification of topological superconductors has proven elusive, it appears that intensive theoretical modeling combined with multiple experimental probes pointing to the same topological state will be needed to reach a definitive conclusion on any given material [13].

In this context, the transition metal dichalcogenide 4Hb-TaS₂ has emerged as a promising candidate for unconventional superconductivity with several experimental studies suggesting the existence of spontaneous time-reversal breaking and/or topological superconductivity [12–17]. Its unit cell is comprised

* raj.a@northeastern.edu

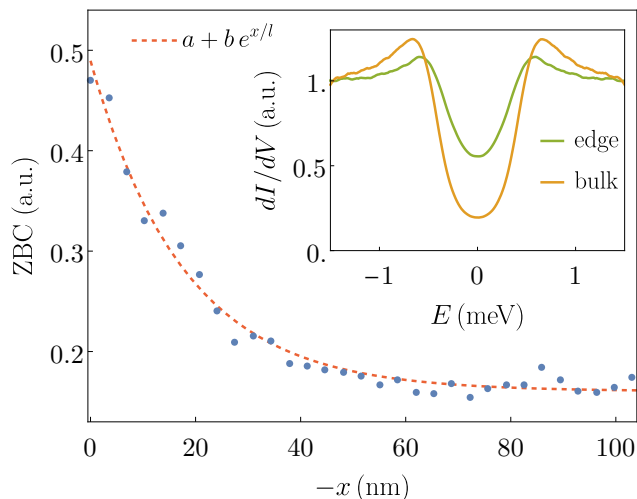


FIG. 1. Experimental results for the 1H step edge reproduced from Ref. [12]. Main panel shows the zero bias peak decaying from the interface at $x = 0$ into the superconducting 1H side ($x < 0$). Dashed red line is a fit to an exponential form with fit parameters: $a = 0.16$, $b = 0.329$, $l = 17.8$ nm. Inset shows the tunneling spectra at the edge and in the bulk.

of an alternate stacking of 1H-TaS₂ and 1T-TaS₂ layers, and the transition temperature is $T_c = 2.7$ K [12, 14, 17]. It is worth noting that while bulk 2H-TaS₂ is a superconductor with a critical temperature of 0.7 K [18], T_c is progressively enhanced for thinner flakes, reaching 2.2 K for 5 layers [19].

Part of the motivation for the expectation of unconventional superconductivity is that 1T-TaS₂ was proposed to host a quantum spin liquid state [20, 21] in bulk crystals. This idea has received support from STM data on monolayers of the closely related compounds 1T-TaSe₂ [22] and 1T-NbSe₂ [23]. Theoretical studies suggest that the ground state of a Hubbard model near the Mott transition is a chiral spin liquid phase [24, 25]. On the other hand, band calculations [26, 27] point to the importance of charge transfer from the 1T to 1H layer in 4Hb bulk crystals, leading to the depletion of local moments and resulting in a metallic state in the 1T layer. There is direct evidence from STM tunneling that this is the case, at least for the top layer [28]. If this continues to be the case in the bulk, the motivation for unconventional pairing in the 1H layers driven by a spin liquid state in the 1T layers is not so clear.

Furthermore, the 4Hb superconductors are known to be in the dirty limit [29], and most known unconventional superconductors usually do not survive in this limit. We note that a recent paper [29] has put forward a conventional explanation for the π phase shift in a Little-Parks experiment for 4Hb-TaS₂ rings [16]. We are therefore motivated to learn if an alternative explanation of the edge tunneling data [12] is possible.

In this work, we treat the 1T layer in the 4Hb compound as a normal metal (assuming screening/charge

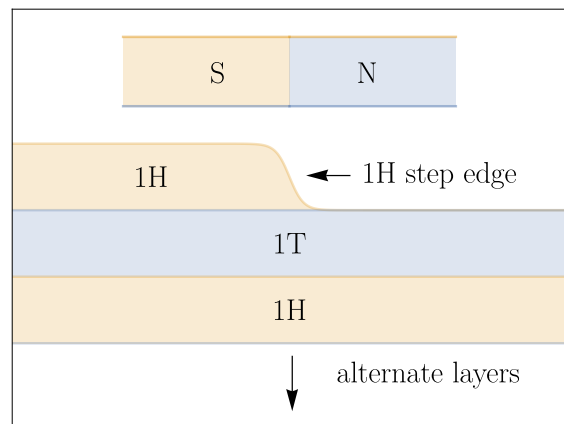


FIG. 2. Schematic of the 1H step edge configuration used in the experiment [12]. Top drawing shows the simplified SN junction geometry we used to model it. Similar experimental results are seen where the role of 1T and 1H are reversed—switching them produces a 1T step edge.

transfer from the adjacent 1H layer [26–28]) and focus on the experimental results of Ref. [12] where a spatially uniform residual DOS is observed within the superconducting gap throughout the 1H surface termination and an exponential rise in the ZBC was seen at the 1H step edge. We have reproduced these results in Fig. 1. The 1H step edge geometry is shown in Fig. 2. To explain these observations, we model the 1H step edge as an SN junction and calculate the dI/dV spectra across it by solving the Usadel equations self-consistently. The model should apply to the experimental configuration shown in Fig. 2 as long as the tunneling between 1T and 1H layers across the step edge dominate over the tunneling between layers in the bulk.

We note that experimentally a similar ZBC was seen in a second geometry where the 1H layer is at the bottom of a crater surrounded by a 1T layer (step edge). We believe our model will also produce similar results for this geometry because quasi-particles will extend from 1T into the 1H layer in the same way, the only difference being that the states under the 1H layer are not accessible to STM tunneling. By varying the phenomenological parameters of the Usadel equations we are able to match many features of the data. We find that a rather broad choice of parameters give similar behavior for the ZBC. Further theoretical studies and additional STM data particularly on the 1T side may be needed to test the applicability of our model.

Our paper is organized as follows. Section II describes the model and the Usadel theory along with features of its non-self-consistent solutions. In Section III, we present and discuss the results of fully self-consistent calculations, focusing on the zero-bias conductance (ZBC) and local density of states (LDOS). In Section IV, we present results that reproduce some features of the data measured in 4Hb-TaS₂. We finish with our main conclusions in Section V.

II. MODEL AND USADEL EQUATIONS

We consider an SN junction with the superconductor on the $x < 0$ side and the normal metal on the $x > 0$ side. The system is taken to be semi-infinite on both the superconducting and normal sides to avoid “mini-gap” features associated with quantum confinement effects from a finite length system on either side of the junction. The superconductor and normal metal have diffusion constants D_S and D_N , respectively. Without any pair breaking terms, the superconductor has a zero-temperature gap of Δ_0 and a transition temperature T_{cS} (we will simply call it T_c). The normal metal is non-superconducting ($T_{cN} = 0$). Unless stated otherwise, the system temperature is taken to be zero. The proximity lengths, $\xi_{S/N} = \sqrt{\hbar D_{S/N}/2\Delta_0}$, define the length scales on the S and N sides.

To study the spatial dependence of Δ and the LDOS across this junction, we use the one-dimensional Usadel equation with inelastic and spin-flip scattering terms, given by [7–9, 30],

$$\frac{\hbar D}{2} \frac{\partial^2 \theta}{\partial x^2} + [iE - \Gamma_{\text{in}} - 2\Gamma_{\text{sf}}(x) \cosh \theta] \sinh \theta - i\Delta(x) \cosh \theta = 0, \quad (1)$$

where $\theta(x, E)$ is a function of the distance to the interface, x , and the energy, E . Here D is the diffusion constant, Γ_{in} is an energy broadening associated with inelastic scattering, and Γ_{sf} is an energy broadening associated with spin flip scattering. While Γ_{in} will be taken to be constant (spatially uniform) throughout the system, various profiles for $\Gamma_{\text{sf}}(x)$ will be considered. The position dependent order parameter, $\Delta(x)$, is obtained from the self-consistency condition [4, 31]:

$$\Delta(x) = NV \int_0^{E_c} dE \tanh\left(\frac{E}{2k_B T}\right) \text{Re}\{\sinh \theta\}. \quad (2)$$

Here E_c is a cutoff energy (\sim Debye energy), N is the normal-state DOS at the Fermi energy (N_S on the S and N_N on the N side) and V is the magnitude of the effective electron-phonon coupling (calculated at zero temperature and without any pair breaking processes) in units such that NV is dimensionless. While V_S is finite, $V_N = 0$ which means $\Delta(x > 0) = 0$. Note that we have chosen the order parameter to be real which is possible for the chosen geometry of the SN junction. From the solution of the Usadel equation, the LDOS, $\rho(x, E)$, is obtained as [8, 9]

$$\rho(x, E) = N \text{Re}\{\cosh(\theta(x, E))\}, \quad (3)$$

and the ZBC is simply $\rho(x, 0)$.

Solving Eq. (1) requires matching the bulk values of θ on the two ends and satisfying additional constraints (for θ and $\partial_x \theta$) at the interface (see Appendix B). For an interface of arbitrary transparency, these constraints

are [32]:

$$\begin{aligned} \sigma_S \left. \frac{\partial \theta(x, E)}{\partial x} \right|_{x=0^-} &= \sigma_N \left. \frac{\partial \theta(x, E)}{\partial x} \right|_{x=0^+} \\ &= \frac{\sinh(\theta(0^+, E) - \theta(0^-, E))}{R_{\text{int}} A_{\text{int}}}, \end{aligned} \quad (4)$$

where σ_S and σ_N are the normal state conductivity of the superconductor and the normal metal, respectively, and R_{int} and A_{int} are the interface resistance and area, respectively. An important dimensionless parameter, γ , which combines $\sigma_{S/N}$ and $D_{S/N}$ is often used to characterize the two systems, and is given by

$$\gamma = \frac{\sigma_N \xi_S}{\sigma_S \xi_N} = \frac{\sigma_N}{\sigma_S} \sqrt{\frac{D_S}{D_N}}. \quad (5)$$

This is known as the mismatch parameter. Another dimensionless parameter

$$\gamma_B = \frac{\sigma_N}{\xi_N} R_{\text{int}} A_{\text{int}} = \gamma \frac{\sigma_S}{\xi_S} R_{\text{int}} A_{\text{int}} \quad (6)$$

is used to characterize the interface transparency. When $\gamma_B = 0$, the interface is perfectly transparent whereas for $\gamma_B \rightarrow \infty$, the S and N sides get decoupled and there are no proximity or inverse-proximity effects. Note that, unless stated otherwise, hereafter x will be in units of ξ_S and ξ_N on the S and N sides, respectively.

A self-consistent solution to the Usadel equation is obtained numerically by an iterative procedure. Features of its solution for a uniform superconductor that are relevant to our study are discussed in Appendix A. For the non-uniform case of an SN junction, details of the numerical method used to solve it are provided in Appendix B. While self-consistent solutions are necessary when one wishes to match theory against experimental data, it is very useful to have a non-self-consistent analytical solution to gain intuition about how various parameters in the model affect the solution. For $\Gamma_{\text{in}} \neq 0$ and $\Gamma_{\text{sf}} = 0$, an analytical solution is provided in Ref [8]. When $\Gamma_{\text{sf}} \neq 0$, such a solution is difficult to obtain for an arbitrary spatial profile of the spin-flip scattering. However, by choosing $\Gamma_{\text{sf}}(x) = \Gamma_{\text{sf}} \Theta(x)$ where $\Theta(x)$ is the Heaviside step function, the Usadel equations on the S and N sides can be linearized and solved analytically for $\gamma_B = 0$ and semi-analytically when γ_B is finite (details given in Appendix C). Note that the technique used here to linearize Eq. (1) on the S side can easily be extended to SS' junctions having only inelastic scattering processes.

For $\gamma_B = 0$, the ZBC on the S and N sides, obtained from the linearized Usadel equations, is given by

$$\frac{\rho(x < 0, 0)}{N_S} = \cos \left[\tan^{-1} \left(\frac{\Delta_0}{\Gamma_{\text{in}}} \right) \left(1 - \frac{e^{-x \sqrt{\Gamma_{\text{in}}^2 + \Delta_0^2}}}{1 + \frac{1}{\gamma} \sqrt{\frac{\Gamma_{\text{in}}^2 + \Delta_0^2}{\Gamma_{\text{in}} + 2\Gamma_{\text{sf}}}}} \right) \right], \quad (7)$$

$$\frac{\rho(x > 0, 0)}{N_N} = \cos \left[\frac{\tan^{-1} \left(\frac{\Delta_0}{\Gamma_{\text{in}}} \right) e^{-x \sqrt{\frac{\Gamma_{\text{in}} + 2\Gamma_{\text{sf}}}{\Delta_0}}}}{1 + \gamma \sqrt{\frac{\Gamma_{\text{in}} + 2\Gamma_{\text{sf}}}{\Gamma_{\text{in}}^2 + \Delta_0^2}}} \right], \quad (8)$$

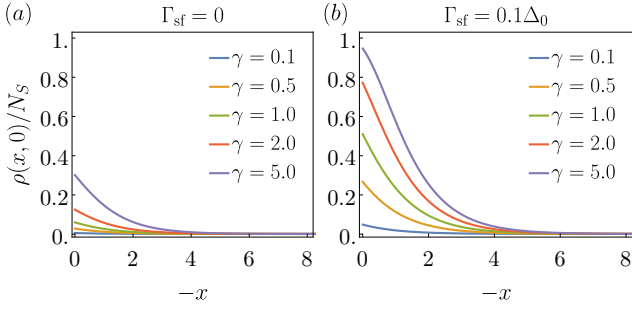


FIG. 3. Spatial variation of the ZBC on the S side without (a), and with (b) a step spin-flip scattering term.

which have bulk values of $N_S/\sqrt{1 + (\Delta_0/\Gamma_{\text{in}})^2}$ and N_N , respectively. We should point out that, based on the self-consistent solution for a uniform superconductor given in Appendix C, increasing Γ_{in} leads to increase in the bulk value of ZBC on the S side until it hits N_S at $\Gamma_{\text{in}} \approx \Delta_0/2$, beyond which superconductivity is completely destroyed and $\rho(x < 0, 0) = N_S$ (see Fig. 11(c)). As seen from Eq. (7), the ZBC rises exponentially as we move from the bulk of S towards the interface, with

$$\frac{\rho(0^-, 0)}{N_S} = \frac{\rho(0^+, 0)}{N_N} = \cos \left[\frac{\tan^{-1} \left(\frac{\Delta_0}{\Gamma_{\text{in}}} \right)}{1 + \gamma \sqrt{\frac{\Gamma_{\text{in}} + 2\Gamma_{\text{sf}}}{\Gamma_{\text{in}}^2 + \Delta_0^2}}} \right]. \quad (9)$$

This clearly shows that increasing γ and/or Γ_{sf} leads to a rise in the ZBC.

For $\gamma_B \neq 0$, the bulk values of the ZBC remain the same as expected. However, γ_B inversely affects the rise in ZBC on the S side, which is easy to understand. Larger γ_B leads to smaller proximity and inverse proximity effects which means that the bulk value of the ZBC on either sides will undergo less change compared to $\gamma_B = 0$ case. This can also be seen from the analytical solutions given in Appendix C. Based on these solutions, we also note that when γ_B is nonzero, $\rho(0^-, 0)/N_S \neq \rho(0^+, 0)/N_N$. This can be a useful guide in deciding whether one needs to consider γ_B when modelling a given experimental data set.

III. RESULTS OF SELF-CONSISTENT CALCULATION

Having gained insights from the non-self-consistent solutions in the previous section, we now present results of self-consistent calculations. Note that, for numerical stability of the self-consistent solution of the Usadel equations, we took a tiny value for the inelastic term, $\Gamma_{\text{in}} = 0.001\Delta_0$, throughout this section. We first consider the case $\gamma_B = 0$. In addition to the step $\Gamma_{\text{sf}}\Theta(x)$, we also consider a Gaussian spin-flip scattering term $\Gamma_{\text{sf}}e^{-bx^2}$.

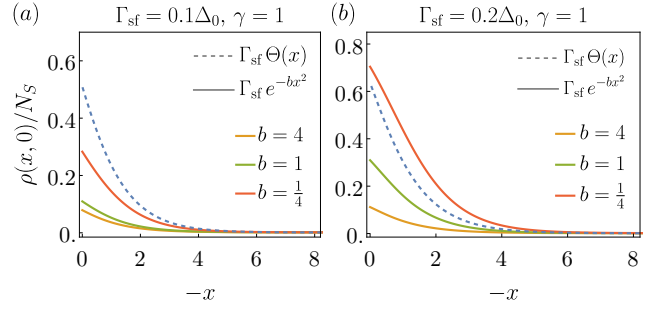


FIG. 4. Comparison between the ZBC on the S side for step and Gaussian spin-flip scattering profiles.

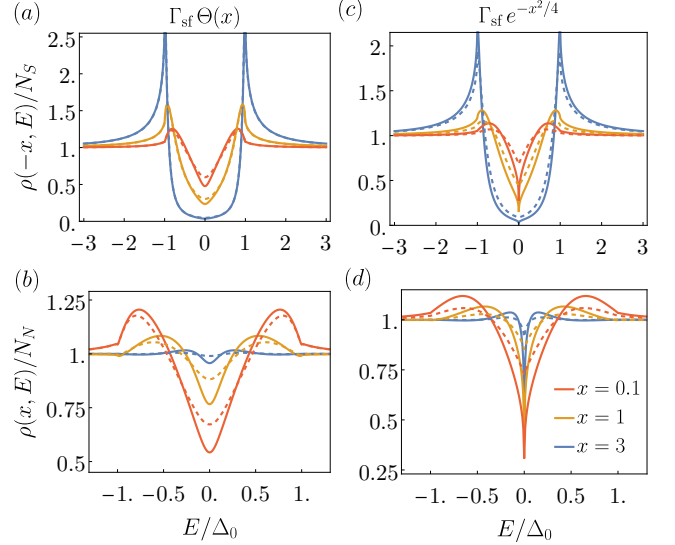


FIG. 5. Comparison between LDOS for $\Gamma_{\text{sf}} = 0.1\Delta_0$ (solid) and $\Gamma_{\text{sf}} = 0.2\Delta_0$ (dashed) on the S side (upper) and N side (lower) for different spatial profiles of the spin-flip scattering term. We have set $\gamma = 1$.

Results for the step profile are shown in Fig. 3 which follows the expected behavior with increasing Γ_{sf} and γ (*i.e.*, an increase in the ZBC). Next, we compare the ZBC for the step and Gaussian profiles for $\gamma = 1$. Results are shown in Fig. 4. We see a significant difference between the Gaussian and step cases, with the former giving rise to a much smaller rise in ZBC compared to the latter unless one takes very large values of Γ_{sf} and small b . A reduction in b causes the spin-flip processes to penetrate further into the S side leading to greater suppression of superconductivity (hence larger increase in ZBC). The difference between these two profiles becomes even more evident from the LDOS plots, shown in Fig. 5. Around $E = 0$, we see an E^2 dependence for ρ in the step case, as predicted from the linearized solution (Appendix C). However, the Gaussian spin-flip term gives rise to a cusp in the LDOS around zero energy. This is not unexpected if we note that for $\Gamma_{\text{in}} = \Gamma_{\text{sf}} = 0$, we get an $\sqrt{|E|}$ behavior near $E = 0$ (Appendix C). Introducing a symmetric or

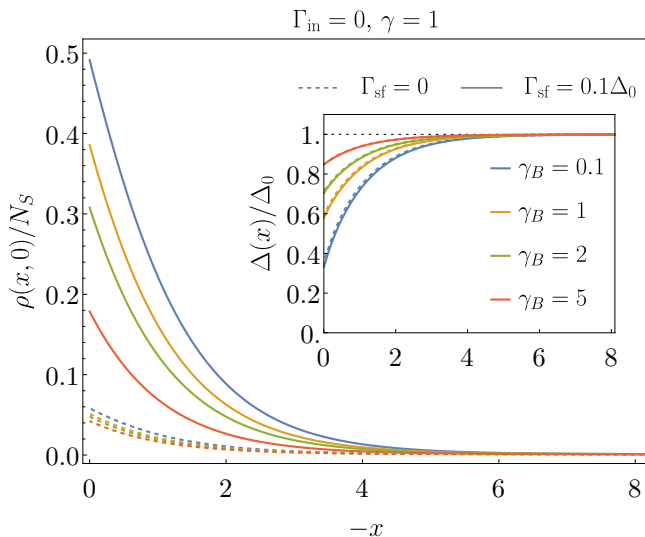


FIG. 6. Effect of interface transparency on the ZBC on the S side, with (solid) and without (dashed) a step-like spin-flip scattering term $\Gamma_{\text{sf}}\Theta(x)$. The inset shows the corresponding self-consistent gap $\Delta(x)$.

interface-localized spin-flip scattering term should not remove this kink while $\Gamma_{\text{in}} = 0$ and Γ_{sf} is not too large.

Finally, we look at the effect of having a partially transparent interface ($\gamma_B \neq 0$). We only consider the step profile here as there is no reason to expect other cases will not show similar behavior with finite γ_B . Results for the ZBC are shown in Fig. 6. As expected, we see a decrease in the ZBC as γ_B is increased. Also, large γ_B leads to reduced proximity and inverse-proximity effects and this is clearly seen from the LDOS plots in Fig. 7.

IV. RESULTS FOR 4Hb-TaS₂

We model the 1H step edge region in Ref. [12] as an SN junction (see Fig. 2) and take $T = 0.38\text{K}$, $\Delta_0 = 0.44\text{meV}$ and $E_c = 100\Delta_0$. As shown in the inset of Fig. 11(a) in Appendix A, one cannot explain the observed ZBC at this temperature while keeping $\Gamma_{\text{in}} = \Gamma_{\text{sf}} = 0$. We take $\Gamma_{\text{in}} = 0.16\Delta_0$, which is about $2k_B T$. This choice of Γ_{in}

TABLE I. Various combinations of $(\gamma_B, \gamma, \Gamma_{\text{sf}})$ that reproduce the experimentally observed rise in ZBC near the 1H step edge at $T = 0.38\text{K}$. We have used a step-like spin-flip scattering term and fixed $\Gamma_{\text{in}} = 0.16\Delta_0$.

γ_B	γ	$\Gamma_{\text{sf}}/\Delta_0$
2	1	0.3
1.3	1	0
0.5	0.5	0.3
0.1	0.5	0.1
0	0.4	0.2
0	0.3	0.5

produces a ZBC of about $0.2N_S$ as is seen in the fit to the symmetrized, averaged, and normalized dI/dV spectra in the bulk of a 1H step (see Fig. 1 or the supplementary of Ref. [12] for more details).

We note that getting this bulk offset in the ZBC by taking a finite Γ_{sf} on the 1H side is also possible but not desirable. As shown in Fig. 11(c) in Appendix A, at low temperatures, the ZBC in the bulk rises sharply in a small region when approaching the critical Γ_{sf} . This will give a tiny bulk value of Δ away from the 1H step-edge which is not seen in the experiment. Keeping this in mind, we will only include a spin-flip scattering term on the 1T side (a step profile). With this setup, we solve the Usadel equation self-consistently for different combinations of the mismatch parameter (γ), the strength of spin-flip scattering (Γ_{sf}) and the boundary transparency (γ_B), and obtain the LDOS using Eq. (3). To compare our results with the experiment, we calculate the differential conductance from ρ using

$$\frac{dI}{dV}(x, \tilde{V}) = - \int_{-\infty}^{+\infty} dE \rho(x, E) \frac{\partial n_F(E - e\tilde{V})}{\partial E}, \quad (10)$$

where $n_F(E) = 1/(1 + e^{E/k_B T})$ is the Fermi function. The ZBC is obtained by setting $\tilde{V} = 0$.

We find that various choices of γ_B , γ and Γ_{sf} produce the reported three-fold exponential rise in the ZBC on the 1H side with a localization length close to the 1H coherence length $\xi = \sqrt{\hbar D_S/\Delta_0} = \sqrt{2}\xi_S$. Some of these values are given in Table I and the corresponding ZBC plots are shown in Fig. 8. These curves compare well with the data shown in Fig. 1. For a select few cases, we have shown the dI/dV spectra at various distances from the interface in Fig. 9. The bulk superconducting gap on the 1H side reduces to about $0.823\Delta_0$ because of the inelastic scattering term. Since we have taken a step like spin-flip scattering term, the dI/dV spectra on the 1H side is predominantly determined by the inelastic scattering rate and temperature. It shows little change between different $(\gamma_B, \gamma, \Gamma_{\text{sf}})$ values from Table I whereas the dI/dV spectra on the 1T side is more sensitive to these parameters. The latter fact can be used to narrow down which set of values better explains the experiment by obtaining more data on the 1T side of the 1H step edge. The set of curves shown in Fig. 9 are in reasonable agreement with the curves shown in the inset in Fig. 1. We should point out that it is also possible to achieve a good agreement with the detailed shape of STM spectra by using a localised $\Gamma_{\text{sf}}(x)$, an example of this is shown in Fig. 10. Thus, even the combination of the ZBC, $\Delta(x)$ around the interface, and the STM spectra does not provide strong constraints on the parameters appearing in the Usadel equations for a good agreement with experiments.

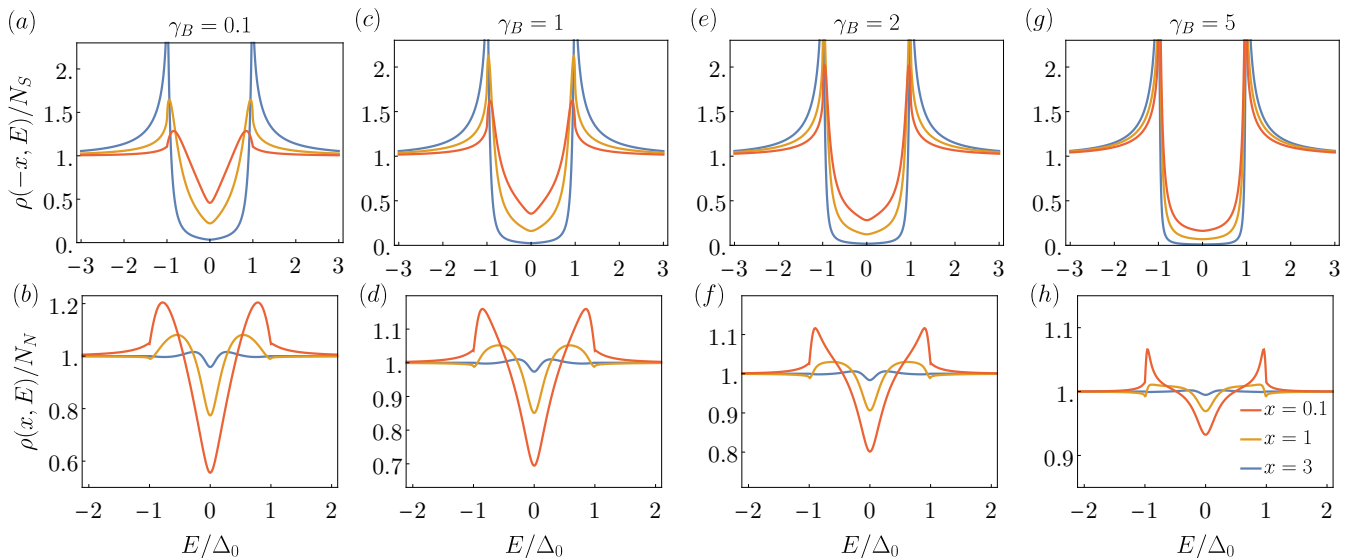


FIG. 7. LDOS on the S side (upper) and N side (lower) for different interface transparency. We have used $\gamma = 1$, $\Gamma_{\text{sf}} = 0.1\Delta_0$.

V. CONCLUSIONS

We have presented a detailed study of the influence of the spatial profile of spin-flip scattering on the ZBC and LDOS in diffusive SN junctions. Our work provides non-self-consistent analytical solutions for the

linearized Usadel equations, focusing on a step-like spin-flip scattering rate $\Gamma_{\text{sf}}\Theta(x)$. We have elucidated the roles of the mismatch parameter γ , the strength of the spin-flip term Γ_{sf} , and the interface transparency γ_B in these systems. Our analysis reveals that increasing γ and Γ_{sf} leads to a more pronounced increase in the ZBC as one approaches the interface from the superconducting side, while γ_B has the opposite effect. We have provided self-consistent calculations to corroborate these findings. Additionally, we have looked at the effects of having localized spin-flip scattering near the interface, offering further insights into the behavior of these junctions for various $\Gamma_{\text{sf}}(x)$.

Furthermore, we have applied our model to the specific case of 4Hb-TaS₂, providing a possible explanation for the observed rise in ZBC in this material. Although our self-consistent solution of the Usadel equations provide a good match for the ZBC and dI/dV spectra, it is important to note that our one-dimensional modeling of the 1H step is highly simplified, leaving ample room for more sophisticated modeling and further exploration into the mechanisms responsible for these observations. For example, it does not predict the different decay lengths of the ZBC away from step edges of different crystallographic orientations.

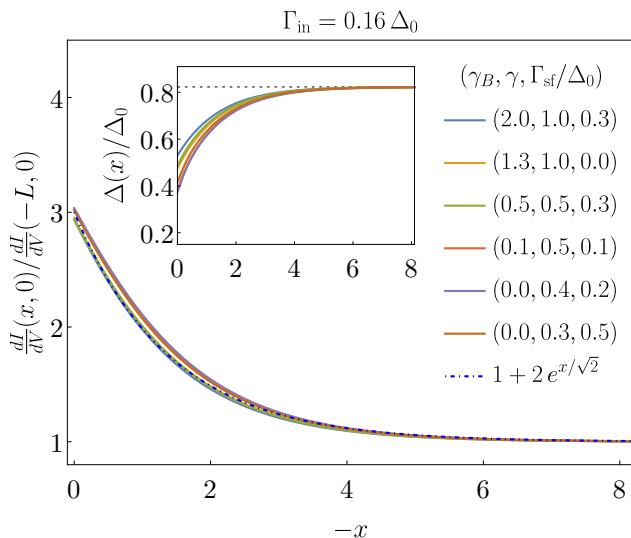


FIG. 8. Zero bias conductance (ZBC) on the 1H side, normalized by its bulk value, for a variety of parameters, but fixing $\Gamma_{\text{in}} = 0.16\Delta_0$. With this choice of Γ_{in} the bulk value is about $0.2056N_S$. We have used $\Gamma_{\text{sf}}\Theta(x)$ as the spin-flip scattering term. The dot-dashed line shows the exponential rise in the ZBC that we wish to reproduce (see Fig. 1). We have used $T = 0.38\text{K}$ and $\Delta_0 = 0.44\text{meV}$. Note that the $\sqrt{2}$ factor appears in the exponential because x is in units of ξ_S and the superconducting coherence length $\xi = \sqrt{2}\xi_S$. The inset shows the self-consistent gap $\Delta(x)$.

VI. ACKNOWLEDGEMENTS

We are grateful to Haim Beidenkopf, Binghai Yan, Yuval Oreg, and Jonathan Ruhman for prior collaborations and discussions on 4Hb-TaS₂. We are especially grateful to Nurit Avraham who helped inspire and initiate this project in addition to participating in important discussions along the way. G.A.F. acknowledges funding from the National

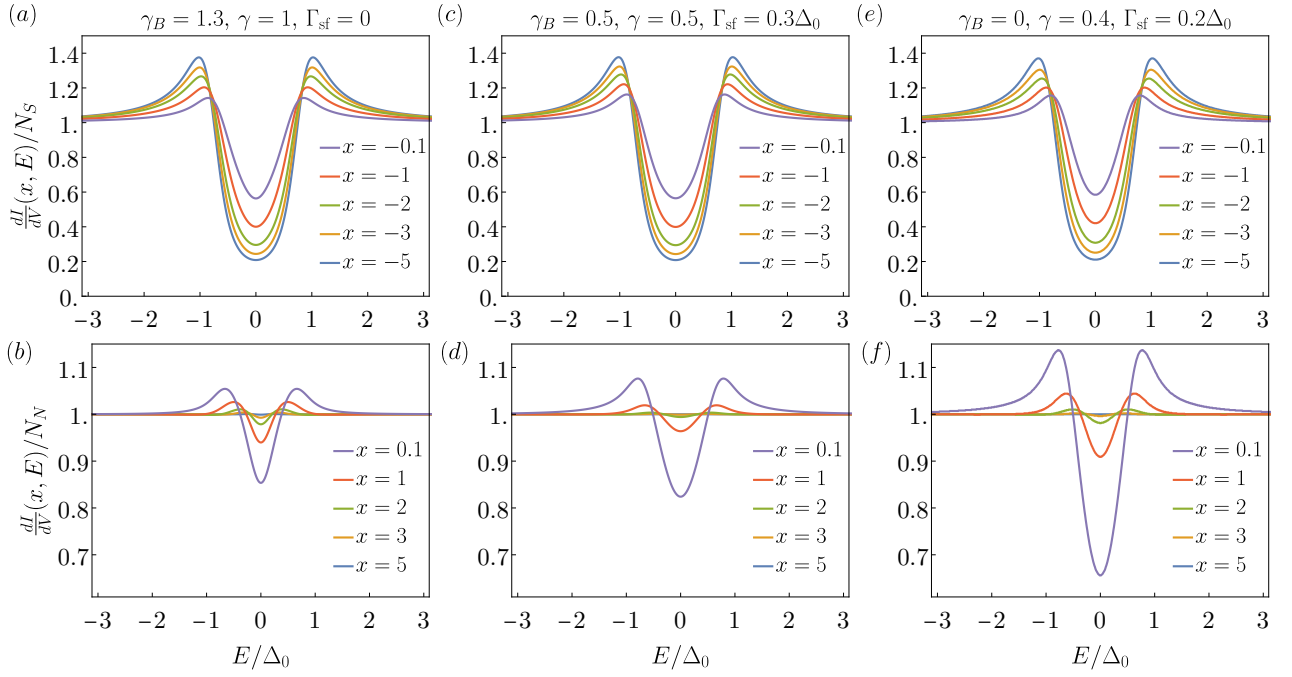


FIG. 9. dI/dV spectra on the 1H side (upper) and 1T side (lower), normalized by its normal-state DOS at Fermi energy, at various distances from the interface. We have taken $\Gamma_{\text{in}} = 0.16\Delta_0$ and $T = 0.38\text{K}$.

Science Foundation through DMR-2114825. G.A.F. acknowledges additional support the Alexander von Humboldt Foundation. PAL acknowledge support by DOE (USA) office of Basic Sciences Grant No. DE-FG02-03ER46076.

Appendix A: Self-consistent solution for a uniform superconductor

For a uniform superconductor, the second-order spatial derivative in Eq. (1) drops out and we get

$$(E + i\Gamma_{\text{in}} + 2i\Gamma_{\text{sf}} \cosh \theta) \sinh \theta = \Delta \cosh \theta. \quad (\text{A1})$$

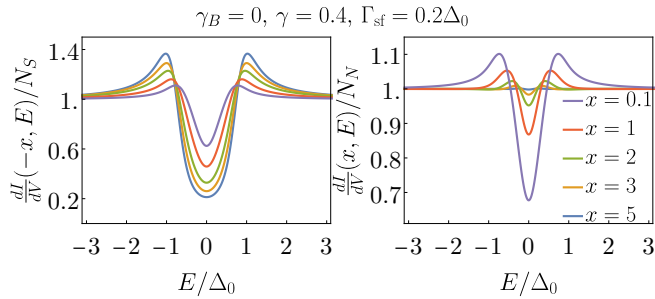


FIG. 10. dI/dV spectra on the 1H (left) and 1T (right) sides for $\Gamma_{\text{sf}}(x) = \Gamma_{\text{sf}} e^{-4x^2}$. We have used $\Gamma_{\text{in}} = 0.16\Delta_0$ and $T = 0.38\text{K}$.

This needs to be solved together with the self-consistency condition given in Eq. (2), which becomes

$$\Delta = N_S V_S \int_0^{E_c} dE \tanh\left(\frac{E}{2k_B T}\right) \text{Re}\{\sinh \theta\}. \quad (\text{A2})$$

Let us look at the case when $\Gamma_{\text{in}} = \Gamma_{\text{sf}} = 0$. At $T = 0$, Δ_0 must be the self-consistent gap parameter. Since $\theta = \tanh^{-1}(\Delta_0/E)$, we can use this to determine $N_S V_S$ from

$$\frac{1}{N_S V_S} = \int_{\Delta_0}^{E_c} \frac{dE}{\sqrt{E^2 - \Delta_0^2}} = \ln\left(\frac{E_c}{\Delta_0} + \sqrt{\frac{E_c^2}{\Delta_0^2} - 1}\right), \quad (\text{A3})$$

which differs from the BCS result only in the negative sign inside both square roots. For $E_c = 100\Delta_0$, this yields $N_S V_S = 0.18874$ (used throughout this paper). We can now find and compare the temperature dependence of Δ with and without pair breaking terms. The plots are shown in Fig. 11(a) and (b), which makes it evident that spin-flip scattering suppresses superconductivity more strongly than the inelastic scattering. This fact is also captured in the inset in Fig. 11(c).

A simple calculation of how large the pair-breaking terms should be to destroy superconductivity at $T = 0$ can be done by noting that as Δ becomes tiny, Eq. (A1) gives $\theta \approx \Delta/(E + i(\Gamma_{\text{in}} + 2\Gamma_{\text{sf}}))$. Putting this in the self-consistency condition we get

$$\frac{1}{N_S V_S} = \int_0^{E_c} dE \text{Re}\left\{\frac{1}{E + i(\Gamma_{\text{in}} + 2\Gamma_{\text{sf}})_c}\right\}, \quad (\text{A4})$$

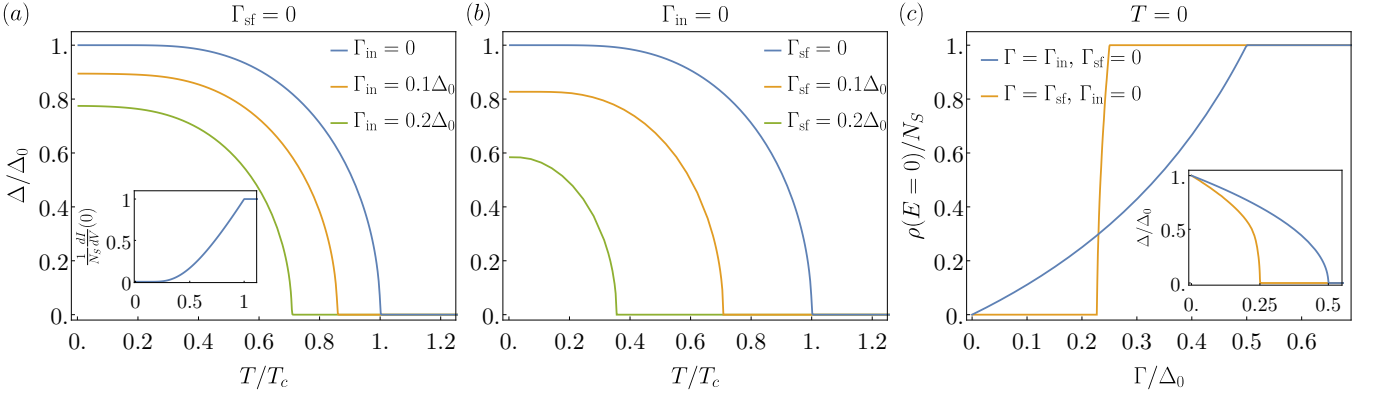


FIG. 11. Self-consistent results for a uniform superconductor. Temperature dependence of Δ in the presence of (a) inelastic scattering, and (b) spin-flip scattering. The ZBC (calculated using Eq. 10) for $\Gamma_{\text{in}} = \Gamma_{\text{sf}} = 0$ is shown in the inset in (a). (c) Dependence of ZBC on Γ_{in} (blue) and Γ_{sf} (orange) at $T = 0$. This was obtained using the corresponding $\Delta(\Gamma)$ curves shown in the inset. We used $E_c = 100\Delta_0$ which gave $N_S V_S = 0.18874$.

where $(\Gamma_{\text{in}} + 2\Gamma_{\text{sf}})_c$ refers to the critical value. Calculating further we get

$$\ln \left(\frac{E_c}{\Delta_0} + \sqrt{\frac{E_c^2}{\Delta_0^2} - 1} \right) = \int_0^{E_c} dE \frac{E}{E^2 + (\Gamma_{\text{in}} + 2\Gamma_{\text{sf}})_c^2}, \quad (\text{A5})$$

$$\Rightarrow \frac{E_c}{\Delta_0} + \sqrt{\frac{E_c^2}{\Delta_0^2} - 1} = \sqrt{\frac{E_c^2 + (\Gamma_{\text{in}} + 2\Gamma_{\text{sf}})_c^2}{(\Gamma_{\text{in}} + 2\Gamma_{\text{sf}})_c^2}}, \quad (\text{A6})$$

$$\Rightarrow (\Gamma_{\text{in}} + 2\Gamma_{\text{sf}})_c \approx \frac{\Delta_0}{2}. \quad (\text{A7})$$

In the last step we used $E_c \gg \Delta_0$. This result also allows us to get $\Gamma_{\text{in},c} \approx \Delta_0/2$ when $\Gamma_{\text{sf}} = 0$ and $\Gamma_{\text{sf},c} \approx \Delta_0/4$ when $\Gamma_{\text{in}} = 0$ (see inset in Fig. 11(c)).

Let us also look at the ZBC for a uniform superconductor at $T = 0$. Let us assume that Δ is the case specific self-consistent superconducting gap in the following. For $0 < \Gamma_{\text{in}} < \Gamma_{\text{in},c}, \Gamma_{\text{sf}} = 0$, $\theta(E = 0) = \tanh^{-1}(\frac{\Delta}{i\Gamma_{\text{in}}})$ which gives a ZBC of $\frac{N_S}{\sqrt{1+(\Delta/\Gamma_{\text{in}})^2}}$. For $\Gamma_{\text{in}} \geq \Gamma_{\text{in},c}$, we get the normal-state DOS N_S at all energies. When $\Gamma_{\text{in}} = 0, 0 < \Gamma_{\text{sf}} < \Gamma_{\text{sf},c}$, $\theta(E = 0) = \sinh^{-1}(\frac{\Delta}{2i\Gamma_{\text{sf}}})$ which gives a ZBC of $N_S \sqrt{1 - (\frac{\Delta}{2\Gamma_{\text{sf}}})^2} \Theta(2\Gamma_{\text{sf}} - \Delta)$. We found that the equality $\Delta = 2\Gamma_{\text{sf}}$ occurs at $\Gamma_{\text{sf}} \approx 0.22797\Delta_0$ for $E_c \gg \Delta_0$. Again, for $\Gamma_{\text{sf}} \geq \Gamma_{\text{sf},c}$, we get the normal-state DOS N_S at all energies. These properties are shown in Fig. 11(c)

Appendix B: Self-consistent solution for SN junctions

Expressing x in units of ξ_S and ξ_N on the S and N sides, respectively, the Usadel equation in Eq. (1) becomes

$$\Delta_0 \frac{\partial^2 \theta_S}{\partial x^2} + [iE - \Gamma_{\text{in}} - 2\Gamma_{\text{sf}}(x) \cosh \theta_S] \sinh \theta_S - i\Delta(x) \cosh \theta_S = 0, \quad (\text{B1})$$

$$\Delta_0 \frac{\partial^2 \theta_N}{\partial x^2} + [iE - \Gamma_{\text{in}} - 2\Gamma_{\text{sf}}(x) \cosh \theta_N] \sinh \theta_N = 0, \quad (\text{B2})$$

where $\theta_S = \theta(x < 0)$ and $\theta_N = \theta(x > 0)$. We will take $-L \leq x \leq L$ and use $L = 100$. To solve this second-order nonlinear differential equation, we set it up as a system of first-order differential equations,

$$\frac{\partial \theta_S}{\partial x} = \phi_S, \quad (\text{B3})$$

$$\frac{\partial \phi_S}{\partial x} = -\frac{1}{\Delta_0} \left([iE - \Gamma_{\text{in}} - 2\Gamma_{\text{sf}}(x) \cosh \theta_S] \sinh \theta_S, -i\Delta(x) \cosh \theta_S \right), \quad (\text{B4})$$

$$\frac{\partial \theta_N}{\partial x} = \phi_N, \quad (\text{B5})$$

$$\frac{\partial \phi_N}{\partial x} = -\frac{1}{\Delta_0} (iE - \Gamma_{\text{in}} - 2\Gamma_{\text{sf}}(x) \cosh \theta_N) \sinh \theta_N. \quad (\text{B6})$$

The problem has boundary conditions both at the two ends and at the SN interface ($x = 0$). This falls under the category of multipoint boundary value problems (BVPs). One way to solve this is to convert it into the usual two-point BVP. To do this, we perform a transformation on the independent variable, $x \rightarrow -x$, on the N side to fold it onto the S side. This also transforms $\theta_N(x, E) \rightarrow \tilde{\theta}_N(x, E) = \theta_N(-x, E)$, and $\phi_N(x, E) \rightarrow \tilde{\phi}_N(x, E) = \phi_N(-x, E)$. We now need to solve a new set of equations but over $[-L, 0]$. This turns the condition at the SN interface into a boundary condition at the right end of the two-point BVP,

$$\frac{\partial \theta_S}{\partial x} = \phi_S, \quad (\text{B7})$$

$$\frac{\partial \phi_S}{\partial x} = -\frac{1}{\Delta_0} \left([iE - \Gamma_{\text{in}} - 2\Gamma_{\text{sf}}(x) \cosh \theta_S] \sinh \theta_S - i\Delta(x) \cosh \theta_S \right), \quad (\text{B8})$$

$$-\frac{\partial \tilde{\theta}_N}{\partial x} = \tilde{\phi}_N, \quad (\text{B9})$$

$$-\frac{\partial \tilde{\phi}_N}{\partial x} = -\frac{1}{\Delta_0} \left(iE - \Gamma_{\text{in}} - 2\Gamma_{\text{sf}}(-x) \cosh \tilde{\theta}_N \right) \sinh \tilde{\theta}_N, \quad (\text{B10})$$

with the boundary conditions:

$$\theta_S(-L, E) = \tanh^{-1} \left[\frac{\Delta(-L)}{E + i\Gamma_{\text{in}}} \right], \quad (\text{B11})$$

$$\tilde{\theta}_N(-L, E) = 0, \quad (\text{B12})$$

$$\phi_S(0, E) = \gamma \tilde{\phi}_N(0, E), \quad (\text{B13})$$

$$\tilde{\phi}_N(0, E) = \frac{1}{\gamma_B} \sinh(\tilde{\theta}_N(0, E) - \theta_S(0, E)). \quad (\text{B14})$$

When $\gamma_B = 0$, the last boundary condition becomes $\tilde{\theta}_N(0, E) = \theta_S(0, E)$, whereas for $\gamma_B \rightarrow \infty$, it gives $\tilde{\phi}_N(0, E) = 0$.

We solve this two-point BVP numerically in Python using the `scipy.integrate.solve_bvp` function, starting with

$$\Delta(x) = \Delta_0. \quad (\text{B15})$$

The the self-consistency condition gives the gap on the S side for the next iteration:

$$\Delta(x) = N_S V_S \int_0^{E_c} dE \tanh\left(\frac{E}{2k_B T}\right) \text{Re} \{ \sinh \theta_S \}. \quad (\text{B16})$$

The procedure is repeated until convergence is achieved, typically within 30 iterations. As before, we use $\Delta_0 = 0.44 \text{ meV}$, $E_c = 100\Delta_0$, and $N_S V_S = 0.18874$.

Appendix C: Solution for linearized Usadel equations

Let us take a step-wise constant gap across the interface,

$$\Delta(x) = \begin{cases} \Delta_0 & \text{if } x < 0 \\ 0 & \text{if } x > 0 \end{cases}. \quad (\text{C1})$$

With this choice, the Usadel equations on the two sides become,

$$\Delta_0 \frac{\partial^2 \theta_S}{\partial x^2} + [iE - \Gamma_{\text{in}}] \sinh \theta_S - i\Delta_0 \cosh \theta_S = 0, \quad (\text{C2})$$

$$\Delta_0 \frac{\partial^2 \theta_N}{\partial x^2} + [iE - \Gamma_{\text{in}} - 2\Gamma_{\text{sf}} \cosh \theta_N] \sinh \theta_N = 0, \quad (\text{C3})$$

where $\theta_S = \theta(x < 0)$ and $\theta_N = \theta(x > 0)$. While the inelastic broadening Γ_{in} is taken to be constant throughout the system, we consider a step-like spin-flip scattering across the interface,

$$\Gamma_{\text{sf}}(x) = \begin{cases} 0 & \text{if } x < 0 \\ \Gamma_{\text{sf}} & \text{if } x > 0 \end{cases}. \quad (\text{C4})$$

We will assume E , Δ_0 , Γ_{in} , and Γ_{sf} to be positive in the remainder of this section.

It is straightforward to linearize Eq.(C3) to

$$\Delta_0 \frac{\partial^2 \theta_N}{\partial x^2} + [iE - \Gamma_{\text{in}} - 2\Gamma_{\text{sf}}] \theta_N = 0, \quad (\text{C5})$$

which is valid for a small θ_N corresponding to a small induced proximity gap. This has a solution of the form

$$\theta_N(x, E) = A(E) e^{-\omega x}, \quad (\text{C6})$$

where $\omega = \sqrt{(-iE + \Gamma_{\text{in}} + 2\Gamma_{\text{sf}})/\Delta_0}$ and A is an unknown function at this moment. We take the principal square root here so that ω has a positive real part.

On the superconducting side of the interface, the order parameter $\Delta(x)$ (and correspondingly $\theta(x, E)$) is not small and one would not expect to be able to expand the Usadel equation around $\theta(x, E) \approx 0$, as was done on the normal side of the interface. However, an expansion around the bulk, uniform superconducting value given by $\theta_0(E) = \tanh^{-1} \left(\frac{\Delta_0}{E + i\Gamma_{\text{in}}} \right)$ should yield sensible results around the interface. We thus substitute

$$\theta_S(x, E) = \theta_0(E) + \delta\theta_S(x, E), \quad (\text{C7})$$

into Eq. (C2) and using

$$\sinh(\theta_0 + \delta\theta_S) \approx \sinh(\theta_0) + \cosh(\theta_0) \delta\theta_S, \quad (\text{C8})$$

$$\cosh(\theta_0 + \delta\theta_S) \approx \cosh(\theta_0) + \sinh(\theta_0) \delta\theta_S, \quad (\text{C9})$$

obtain (to linear order in $\delta\theta_S$)

$$\Delta_0 \frac{\partial^2 \delta\theta_S}{\partial x^2} + [iE - \Gamma_{\text{in}}] \cosh(\theta_0) \delta\theta_S - i\Delta_0 \sinh(\theta_0) \delta\theta_S = 0, \quad (\text{C10})$$

which simplifies to

$$\Delta_0 \frac{\partial^2 \delta\theta_S}{\partial x^2} + i \sqrt{(E + i\Gamma_{\text{in}})^2 - \Delta_0^2} \delta\theta_S = 0. \quad (\text{C11})$$

Similar to the N side, it has a solution of the form

$$\delta\theta_S(x, E) = B(E) e^{\omega' x}, \quad (\text{C12})$$

where $\omega' = \sqrt{-i \sqrt{(E + i\Gamma_{\text{in}})^2 / \Delta_0^2 - 1}}$ (we take the principal square root at both levels so that ω' is guaranteed to have a positive real part) and B is another unknown function. We determine A and B from the condition at the interface.

Assuming perfect transparency ($\gamma_B = 0$), the condition on θ at the interface gives

$$A = \theta_0 + B. \quad (\text{C13})$$

Similarly, the condition on its derivative gives

$$-\gamma\omega A = \omega' B. \quad (\text{C14})$$

We solve for A and B to get:

$$A = \frac{\theta_0}{1 + \gamma\omega/\omega'} \quad (\text{C15})$$

$$B = \frac{-\theta_0}{1 + \omega'/\gamma\omega}. \quad (\text{C16})$$

Thus, we obtain the following solution for the linearized Usadel equation

$$\theta_S(x, E) = \theta_0 - \frac{\theta_0}{1 + \omega'/\gamma\omega} e^{\omega'x}, \quad x \leq 0 \quad (\text{C17})$$

$$\theta_N(x, E) = \frac{\theta_0}{1 + \gamma\omega/\omega'} e^{-\omega x}, \quad x \geq 0. \quad (\text{C18})$$

It is straightforward to obtain the LDOS from this as,

$$\rho(x, E) = \begin{cases} N_S \operatorname{Re}\{\cosh(\theta_S)\} & \text{if } x < 0 \\ N_N \operatorname{Re}\{\cosh(\theta_N)\} & \text{if } x > 0 \end{cases}. \quad (\text{C19})$$

1. LDOS for $E \ll \Delta_0$ when $\Gamma_{\text{in}} = \Gamma_{\text{sf}} = 0$

In absence of any pair-breaking scattering mechanisms, the LDOS near $E = 0$ is given by

$$\rho(x, E) \approx \begin{cases} \frac{N_S \pi}{2\sqrt{2}} \gamma e^x \sqrt{\frac{|E|}{\Delta_0}}, & x < 0 \\ \frac{N_N \pi}{2\sqrt{2}} (\gamma + x) \sqrt{\frac{|E|}{\Delta_0}}, & x > 0 \end{cases}, \quad (\text{C20})$$

and shows a $\sqrt{|E|}$ dependence. Note that if one uses the non-self-consistent analytical solution from [8], the factor $\frac{\pi}{2\sqrt{2}}$ drops out.

2. LDOS for $E \ll \Delta_0$ when $\Gamma_{\text{in}} + \Gamma_{\text{sf}} \neq 0$

When either of Γ_{in} , Γ_{sf} is nonzero ($\Gamma_{\text{in}} + \Gamma_{\text{sf}} \neq 0$), the LDOS is given by

$$\rho(x, E) \approx \begin{cases} N_S \cos \left(\tan^{-1} \left(\frac{\Delta_0}{\Gamma_{\text{in}}} \right) \frac{1 + \gamma \sqrt{\frac{\Gamma_{\text{in}} + 2\Gamma_{\text{sf}}}{\sqrt{\Gamma_{\text{in}}^2 + \Delta_0^2}}} \left(1 - e^{x \sqrt{1 + \Gamma_{\text{in}}^2 / \Delta_0^2}} \right)}{1 + \gamma \sqrt{\frac{\Gamma_{\text{in}} + 2\Gamma_{\text{sf}}}{\sqrt{\Gamma_{\text{in}}^2 + \Delta_0^2}}}} \right) \left(1 + \mathcal{O} \left(\frac{E^2}{\Delta_0^2} \right) \right), & x < 0 \\ N_N \cos \left(\tan^{-1} \left(\frac{\Delta_0}{\Gamma_{\text{in}}} \right) \frac{e^{-x \sqrt{(\Gamma_{\text{in}} + 2\Gamma_{\text{sf}}) / \Delta_0}}}{1 + \gamma \sqrt{\frac{\Gamma_{\text{in}} + 2\Gamma_{\text{sf}}}{\sqrt{\Gamma_{\text{in}}^2 + \Delta_0^2}}}} \right) \left(1 + \mathcal{O} \left(\frac{E^2}{\Delta_0^2} \right) \right), & x > 0 \end{cases}, \quad (\text{C21})$$

which has a finite value at $E = 0$ and follows a E^2 dependence. Let us explicitly calculate the ZBC on the N and S sides of the interface. For the N side we get

$$\frac{\rho(x > 0, 0)}{N_N} = \cos \left[\frac{\tan^{-1} \left(\frac{\Delta_0}{\Gamma_{\text{in}}} \right) e^{-x \sqrt{\frac{\Gamma_{\text{in}} + 2\Gamma_{\text{sf}}}{\Delta_0}}}}{1 + \gamma \sqrt{\frac{\Gamma_{\text{in}} + 2\Gamma_{\text{sf}}}{\sqrt{\Gamma_{\text{in}}^2 + \Delta_0^2}}}} \right], \quad (\text{C22})$$

which has a bulk value of $\rho(+\infty, 0) = N_N$, as expected. Similarly, the ZBC on S side is given by

$$\frac{\rho(x < 0, 0)}{N_S} = \cos \left[\tan^{-1} \left(\frac{\Delta_0}{\Gamma_{\text{in}}} \right) \left(1 - \frac{e^{x \sqrt{1 + \Gamma_{\text{in}}^2 / \Delta_0^2}}}{1 + \frac{1}{\gamma} \sqrt{\frac{\Gamma_{\text{in}} + 2\Gamma_{\text{sf}}}{\sqrt{\Gamma_{\text{in}}^2 + \Delta_0^2}}}} \right) \right] \quad (\text{C23})$$

and has the bulk value

$$\rho(-\infty, 0) = \frac{N_S}{\sqrt{1 + (\Delta_0/\Gamma_{\text{in}})^2}}. \quad (\text{C24})$$

At the interface, we find that

$$\frac{\rho(0^-, 0)}{N_S} = \frac{\rho(0^+, 0)}{N_N} = \cos \left[\frac{\tan^{-1} \left(\frac{\Delta_0}{\Gamma_{\text{in}}} \right)}{1 + \gamma \sqrt{\frac{\Gamma_{\text{in}} + 2\Gamma_{\text{sf}}}{\sqrt{\Gamma_{\text{in}}^2 + \Delta_0^2}}}} \right], \quad (\text{C25})$$

which is always nonzero for $\Gamma_{\text{in}} + \Gamma_{\text{sf}} \neq 0$.

3. Solution for $\gamma_B \neq 0$

When $\gamma_B \neq 0$, the boundary conditions give

$$\omega' B = -\gamma\omega A = \frac{\gamma}{\gamma_B} \sinh(A - B - \theta_0) \quad (\text{C26})$$

and we obtain

$$\theta_S(x, E) = \theta_0 - \frac{\gamma\omega A}{\omega'} e^{\omega'x}, \quad x < 0 \quad (\text{C27})$$

$$\theta_N(x, E) = A e^{-\omega x}, \quad x > 0 \quad (\text{C28})$$

where, $A(E)$ needs to be found numerically for an arbitrary value of γ_B by solving

$$\gamma_B \omega A = \sinh\left(\theta_0 - A\left(1 + \frac{\gamma\omega}{\omega'}\right)\right). \quad (\text{C29})$$

However, we can get an approximate solution for A in two extreme limits. Let us first consider the case $\gamma_B \ll 1$. This condition allows us to simplify Eq. (C29) to get

$$A \approx \frac{\theta_0}{1 + \gamma\omega/\omega' + \gamma_B\omega}. \quad (\text{C30})$$

From this, we calculate the ZBC

$$\frac{\rho(x > 0, 0)}{N_N} = \cos \left[\frac{\tan^{-1}\left(\frac{\Delta_0}{\Gamma_{\text{in}}}\right) e^{-x\sqrt{\frac{\Gamma_{\text{in}}+2\Gamma_{\text{sf}}}{\Delta_0}}}}{1 + \gamma\sqrt{\frac{\Gamma_{\text{in}}+2\Gamma_{\text{sf}}}{\sqrt{\Gamma_{\text{in}}^2+\Delta_0^2}}} + \gamma_B\sqrt{\frac{\Gamma_{\text{in}}+2\Gamma_{\text{sf}}}{\Delta_0}}} \right], \quad (\text{C31})$$

$$\frac{\rho(x < 0, 0)}{N_S} = \cos \left[\tan^{-1}\left(\frac{\Delta_0}{\Gamma_{\text{in}}}\right) - \frac{\tan^{-1}\left(\frac{\Delta_0}{\Gamma_{\text{in}}}\right) e^{x\sqrt{1+\Gamma_{\text{in}}^2/\Delta_0^2}}}{1 + \frac{1}{\gamma}\sqrt{\frac{\sqrt{\Gamma_{\text{in}}^2+\Delta_0^2}}{\Gamma_{\text{in}}+2\Gamma_{\text{sf}}}} + \frac{\gamma_B}{\gamma}\sqrt{\frac{\sqrt{\Gamma_{\text{in}}^2+\Delta_0^2}}{\Delta_0}}} \right]. \quad (\text{C32})$$

Similarly, when $\gamma_B \gg 1$, Eq. (C29) simplifies to

$$A \approx \frac{\tanh(\theta_0)}{1 + \gamma\omega/\omega' + i\gamma_B\omega\omega'^2 \tanh(\theta_0)} \approx \frac{1}{i\gamma_B\omega\omega'^2} \quad (\text{C33})$$

which gives the ZBC

$$\frac{\rho(x > 0, 0)}{N_N} = \cos \left[\frac{e^{-x\sqrt{\frac{\Gamma_{\text{in}}+2\Gamma_{\text{sf}}}{\Delta_0}}}}{\gamma_B\sqrt{\frac{\Gamma_{\text{in}}+2\Gamma_{\text{sf}}}{\Delta_0}}\sqrt{\frac{\Gamma_{\text{in}}^2+\Delta_0^2}{\Delta_0}}} \right], \quad (\text{C34})$$

$$\frac{\rho(x < 0, 0)}{N_S} = \cos \left[\tan^{-1}\left(\frac{\Delta_0}{\Gamma_{\text{in}}}\right) - \frac{e^{x\sqrt{1+\Gamma_{\text{in}}^2/\Delta_0^2}}}{\frac{\gamma_B}{\gamma}\left(1 + \frac{\Gamma_{\text{in}}^2}{\Delta_0^2}\right)^{3/4}} \right]. \quad (\text{C35})$$

In both limits, an increase in γ_B leads to decrease in $\rho(0^-, 0)$ and increase in $\rho(0^+, 0)$. Also note that for a nonzero γ_B ,

$$\frac{\rho(0^-, 0)}{N_S} \neq \frac{\rho(0^+, 0)}{N_N}. \quad (\text{C36})$$

-
- [1] P. G. De Gennes, Boundary effects in superconductors, *Rev. Mod. Phys.* **36**, 225 (1964).
- [2] B. Pannetier and H. Courtois, Andreev reflection and proximity effect, *Journal of low temperature physics* **118**, 599 (2000).
- [3] S. Guéron, H. Pothier, N. O. Birge, D. Esteve, and M. H. Devoret, Superconducting proximity effect probed on a mesoscopic length scale, *Phys. Rev. Lett.* **77**, 3025 (1996).
- [4] N. Moussy, H. Courtois, and B. Pannetier, Local spectroscopy of a proximity superconductor at very low temperature, *Europhysics Letters (EPL)* **55**, 861 (2001).
- [5] M. Vinet, C. Chapelier, and F. Lefloch, Spatially resolved spectroscopy on superconducting proximity nanostructures, *Phys. Rev. B* **63**, 165420 (2001).
- [6] M. Meschke, J. T. Peltonen, J. P. Pekola, and F. Giazotto, Tunnel spectroscopy of a proximity josephson junction, *Phys. Rev. B* **84**, 214514 (2011).
- [7] K. D. Usadel, Generalized diffusion equation for superconducting alloys, *Phys. Rev. Lett.* **25**, 507 (1970).
- [8] W. Belzig, C. Bruder, and G. Schön, Local density of states in a dirty normal metal connected to a superconductor, *Phys. Rev. B* **54**, 9443 (1996).
- [9] B. Crouzy, E. Bascones, and D. A. Ivanov, Minigap in a superconductor–normal metal junction with paramagnetic impurities, *Phys. Rev. B* **72**, 092501 (2005).
- [10] A. A. Golubov, F. K. Wilhelm, and A. D. Zaikin, Coherent charge transport in metallic proximity structures, *Phys. Rev. B* **55**, 1123 (1997).
- [11] S. Yip, Conductance anomalies for normal-metal–insulator–superconductor contacts, *Phys. Rev. B* **52**, 15504 (1995).
- [12] A. K. Nayak, A. Steinbok, Y. Roet, J. Koo, G. Margalit, I. Feldman, A. Almoalem, A. Kanigel, G. A. Fiete, B. Yan, *et al.*, Evidence of topological boundary modes with topological nodal-point superconductivity, *Nature physics* **17**, 1413 (2021).
- [13] A. Raj, A. Postlewaite, S. Chaudhary, and G. A. Fiete, Nonlinear optical responses in multiorbital topological superconductors, *Phys. Rev. B* **109**, 184514 (2024).
- [14] A. Ribak, R. M. Skiff, M. Mograbi, P. Rout, M. Fischer, J. Ruhman, K. Chashka, Y. Dagan, and A. Kanigel, Chiral superconductivity in the alternate stacking compound 4Hb-TaS₂, *Science advances* **6**, eaax9480 (2020).
- [15] E. Persky, A. V. Bjørlig, I. Feldman, A. Almoalem, E. Altman, E. Berg, I. Kimchi, J. Ruhman, A. Kanigel, and B. Kalisky, Magnetic memory and spontaneous vortices in a van der Waals superconductor, *Nature* **607**, 692 (2022).
- [16] A. Almoalem, I. Feldman, M. Shlafman, Y. E. Yaish, M. H. Fischer, M. Moshe, J. Ruhman, and A. Kanigel, Evidence of a two-component order parameter in 4Hb-TaS₂ in the little-parks effect, *arXiv preprint arXiv:2208.13798* (2022).
- [17] I. Silber, S. Mathimalar, I. Mangel, A. Nayak, O. Green, N. Avraham, H. Beidenkopf, I. Feldman, A. Kanigel, A. Klein, *et al.*, Two-component nematic superconductivity in 4Hb-TaS₂, *Nature Communications*

- 15**, 824 (2024).
- [18] S. Nagata, T. Aochi, T. Abe, S. Ebisu, T. Hagino, Y. Seki, and K. Tsutsumi, Superconductivity in the layered compound 2H-TaS₂, *Journal of Physics and Chemistry of Solids* **53**, 1259 (1992).
- [19] E. Navarro-Moratalla, J. O. Island, S. Manas-Valero, E. Pinilla-Cienfuegos, A. Castellanos-Gomez, J. Quereda, G. Rubio-Bollinger, L. Chirolli, J. A. Silva-Guillén, N. Agraït, *et al.*, Enhanced superconductivity in atomically thin TaS₂, *Nature communications* **7**, 11043 (2016).
- [20] K. T. Law and P. A. Lee, 1T-TaS₂ as a quantum spin liquid, *Proceedings of the National Academy of Sciences* **114**, 6996 (2017).
- [21] W.-Y. He, X. Y. Xu, G. Chen, K. T. Law, and P. A. Lee, Spinon fermi surface in a cluster mott insulator model on a triangular lattice and possible application to 1T-TaS₂, *Physical review letters* **121**, 046401 (2018).
- [22] W. Ruan, Y. Chen, S. Tang, J. Hwang, H.-Z. Tsai, R. L. Lee, M. Wu, H. Ryu, S. Kahn, F. Liou, *et al.*, Evidence for quantum spin liquid behaviour in single-layer 1T-TaSe₂ from scanning tunnelling microscopy, *Nature Physics* **17**, 1154 (2021).
- [23] Q. Zhang, W.-Y. He, Y. Zhang, Y. Chen, L. Jia, Y. Hou, H. Ji, H. Yang, T. Zhang, L. Liu, *et al.*, Quantum spin liquid signatures in monolayer 1T-NbSe₂, *Nature Communications* **15**, 2336 (2024).
- [24] W.-J. Hu, S.-S. Gong, and D. Sheng, Variational monte carlo study of chiral spin liquid in quantum antiferromagnet on the triangular lattice, *Physical Review B* **94**, 075131 (2016).
- [25] A. Szasz, J. Motruk, M. P. Zaletel, and J. E. Moore, Chiral spin liquid phase of the triangular lattice hubbard model: A density matrix renormalization group study, *Physical Review X* **10**, 021042 (2020).
- [26] L. Crippa, H. Bae, P. Wunderlich, I. I. Mazin, B. Yan, G. Sangiovanni, T. Wehling, and R. Valentí, Heavy fermions vs doped mott physics in heterogeneous Ta-dichalcogenide bilayers, *Nature Communications* **15**, 1357 (2024).
- [27] C. Wen, J. Gao, Y. Xie, Q. Zhang, P. Kong, J. Wang, Y. Jiang, X. Luo, J. Li, W. Lu, Y.-P. Sun, and S. Yan, Roles of the narrow electronic band near the fermi level in 1T-TaS₂-related layered materials, *Phys. Rev. Lett.* **126**, 256402 (2021).
- [28] A. Kumar Nayak, A. Steinbok, Y. Roet, J. Koo, I. Feldman, A. Almoalem, A. Kanigel, B. Yan, A. Rosch, N. Avraham, *et al.*, First-order quantum phase transition in the hybrid metal-mott insulator transition metal dichalcogenide 4Hb-TaS₂, *Proceedings of the National Academy of Sciences* **120**, e2304274120 (2023).
- [29] M. H. Fischer, P. A. Lee, and J. Ruhman, Mechanism for π phase shifts in little-parks experiments: Application to 4Hb-TaS₂ and to 2H-TaS₂ intercalated with chiral molecules, *Phys. Rev. B* **108**, L180505 (2023).
- [30] J. C. Hammer, J. C. Cuevas, F. S. Bergeret, and W. Belzig, Density of states and supercurrent in diffusive sns junctions: Roles of nonideal interfaces and spin-flip scattering, *Phys. Rev. B* **76**, 064514 (2007).
- [31] V. Cherkez, J. C. Cuevas, C. Brun, T. Cren, G. Ménard, F. Debontridder, V. S. Stolyarov, and D. Roditchev, Proximity effect between two superconductors spatially resolved by scanning tunneling spectroscopy, *Phys. Rev. X* **4**, 011033 (2014).
- [32] M. Y. Kuprianov and V. Lukichev, Influence of boundary transparency on the critical current of “dirty” ss’s structures, *Zh. Eksp. Teor. Fiz* **94**, 139 (1988).